

JGR Space Physics

TECHNICAL REPORTS: METHODS

10.1029/2021JA029263

Key Points:

- We develop a novel technique to determine electron densities in Jupiter's magnetosphere
- We describe how appropriate characteristic frequencies can be identified and digitized from plasma wave spectra
- We provide expected uncertainties for the density and some caveats for use

Correspondence to:

A. H. Sulaiman,
ali-sulaiman@uiowa.edu






Citation:

Sulaiman, A. H., Elliott, S. S., Kurth, W. S., Faden, J. B., Hospodarsky, G. B., & Menietti, J. D. (2021). Inferring Jovian electron densities using plasma wave spectra obtained by the Juno/Waves instrument. *Journal of Geophysical Research: Space Physics*, 126, e2021JA029263. <https://doi.org/10.1029/2021JA029263>

Received 19 FEB 2021

Accepted 31 MAY 2021

Inferring Jovian Electron Densities Using Plasma Wave Spectra Obtained by the Juno/Waves Instrument

A. H. Sulaiman¹ , S. S. Elliott¹ , W. S. Kurth¹ , J. B. Faden¹, G. B. Hospodarsky¹ , and J. D. Menietti¹ 

¹Department of Physics and Astronomy, University of Iowa, Iowa City, IA, USA

Abstract The Waves instrument onboard the Juno spacecraft has plasma wave-measuring capabilities using a single electric dipole antenna and a uniaxial magnetic search coil. Together, these simultaneously measure electric and magnetic field spectral densities in the frequency range 50 Hz–20 kHz, above which only electric field spectral densities are measured up to 41 MHz. A major objective of the Juno mission is to explore Jupiter's high-latitude magnetosphere and ionosphere. One of the key contributions of the Waves instrument is the determination of electron densities from plasma wave spectra. Given the very high magnetic field strengths near Juno's perijove passes, established techniques cannot be utilized to infer electron densities since such highly magnetized space plasma conditions have not previously been met in planetary missions. By revisiting theoretical treatments of plasma waves, we describe a novel method to determine electron densities from plasma wave spectra that is unique to the near-Jupiter region. In the absence of the commonly observed upper hybrid resonance frequency in high-density space plasmas (e.g., the vicinities of Io, Ganymede, Enceladus, and the near-Earth environment), we achieve this by identifying emission cutoffs at the lower hybrid frequency and electron plasma frequency. Further, we discuss the development of the process and tools for identifying and digitizing appropriate resonance and cutoff frequencies.

1. Introduction

The plasma density is a fundamental property necessary for understanding and modeling various space plasma and planetary phenomena including, but not limited to, (a) plasma wave generation, growth, and propagation, (b) the structure and dynamics of the ionosphere and magnetosphere (if present) of planets and satellites, and (c) auroral processes. Herein, we specifically discuss inferring the electron number density, n_e , which may be used on its own, or to constrain ion densities where quasi-neutrality holds.

Plasma wave measurements are not susceptible to the challenges that particle-counting plasma instruments must deal with. Nonzero spacecraft potentials, pointing constraints, and the adverse effects of penetrating radiation often limit particle-counting plasma instruments from capturing the full particle distribution, necessary to deriving densities. Plasma wave measurements, on the other hand, can infer the electron density from measured plasma wave oscillations and/or clear frequency cutoffs that are functions of the electron number density. Electron plasma oscillations at the electron plasma frequency, f_{pe} , are canonically used to derive n_e through the relationship

$$f_{pe} = \frac{1}{2\pi} \sqrt{\frac{n_e e^2}{m_e \epsilon_0}} \quad (1)$$

where e is the electric charge, m_e is the electron mass, and ϵ_0 is the permittivity of free space. Note that f_{pe} is calculated as real frequency measured in hertz. This relationship can be approximated as

$$n_e [\text{cm}^{-3}] \approx \left(\frac{f_{pe} [\text{Hz}]}{8980} \right)^2 \quad (2)$$

This approximation is valid in the cold plasma limit where the oscillations are non-propagating and dispersionless. This is typically the case in the solar wind where Langmuir waves are present upstream of the bow shock (e.g., Hospodarsky et al., 2017) and regions in a magnetosphere where plasma temperatures are low.

Often in dense environments such as the Earth's plasmasphere or the orbits of Enceladus and Io, the upper hybrid frequency, f_{UH} , appears as a narrowband emission (Gurnett et al., 1996a, 1996b; Kurth et al., 2015; Persoon et al., 2005). This can be used to derive the electron density as $f_{UH}^2 = f_{pe}^2 + f_{ce}^2$, where f_{ce} is the electron cyclotron frequency calculated from the magnetic field strength B using a magnetometer as f_{ce} [Hz] $\approx 28|B|$ [nT].

Quasi-thermal noise spectroscopy is another method used to determine electron density, in addition to temperatures and bulk velocity. This is a result of the interaction of the antenna with the ambient plasma (Meyer-Vernet & Perche, 1989). This method is used with long-dipole antennas with a length that satisfies $L \gg \lambda_D$, the Debye length.

In this article, we will introduce methods for inferring electron densities appropriate for the near-Jupiter environment, a regime unique in solar system planetary environments that is characterized by an ultra-high magnetic field strength. Such highly magnetized regimes are typically attained in the solar corona but not usually in planetary environments. By identifying common wave modes using the Waves instrument on-board Juno (Kurth et al., 2017), we will demonstrate how their cutoffs at characteristic frequencies can be used to derive the electron plasma frequency, and hence the electron density. This novel method is necessary because, as will be shown in the next section, the approximations commonly used for hybrid frequencies do not hold in this previously unexplored regime where $f_{pe}/f_{ce} \ll 1$.

2. Using Juno/Waves Plasma Wave Observations to Determine n_e

2.1. Theoretical Background

We consider the various fundamental and derived characteristic frequencies in the cold plasma approximation (Gurnett & Bhattacharjee, 2017; Stix, 1992). A parameter space of the characteristic frequencies is shown in Figure 1. The independent variable is chosen, without loss of generality, as the ratio of the electron plasma to cyclotron frequencies, f_{pe}/f_{ce} . In the direction of increasing f_{pe}/f_{ce} , the plasma regime is of higher density (or low magnetized), and conversely in the direction of decreasing f_{pe}/f_{ce} , the plasma regime is of lower density (or highly magnetized). Spanning many orders of magnitude, the parameter space covers a variety of regimes in the solar system, for example, Earth's plasmasphere ($f_{pe}/f_{ce} \gg 1$) (Meredith et al., 2003), the orbits of Enceladus and Io ($f_{pe}/f_{ce} > 1$) (Gurnett et al., 1996b; Persoon et al., 2005), Ganymede's magnetosphere ($f_{pe}/f_{ce} \sim 1$) (Gurnett et al., 1996a), Saturn's ionosphere ($f_{pe}/f_{ce} \sim 1$) (Persoon et al., 2019; Sulaiman et al., 2017), and Jupiter's inner magnetosphere and ionosphere ($f_{pe}/f_{ce} \ll 1$).

The curves in Figure 1 are solutions to elements of the dielectric tensor for waves in a cold uniform proton-electron magnetized plasma, as defined by Stix (1992) and Gurnett and Bhattacharjee (2017). These are R and L for the derivation of the right- and left-hand mode cutoff frequencies, respectively, and more importantly S for the derivation of hybrid frequencies. The significance of S is that there exist two solutions, namely the upper hybrid, f_{UH} , and lower hybrid, f_{LH} , frequencies—both of which are functions of f_{pe} and therefore the electron density. The S equation for a proton-electron plasma is written as

$$S = 1 - \sum_s \frac{f_{ps}^2}{f^2 - f_{cs}^2} = 1 - \frac{f_{pe}^2}{f^2 - f_{ce}^2} - \frac{f_{pH+}^2}{f^2 - f_{cH+}^2} = 0 \quad (3)$$

where f_p and f_c are the plasma and cyclotron frequencies, respectively, and the subscript s denotes the species.

One method of inferring f_{pe} is from the lower hybrid frequency, f_{LH} , (blue curve) which can be identified in a spectrogram as the lower frequency limit of broadband whistler-mode emissions (Gurnett & Bhattacharjee, 2017; LaBelle & Treumann, 2002). Unlike f_{UH} which is analytically expressed as $(f_{pe}^2 + f_{ce}^2)^{1/2}$ regardless of how over/under dense the plasma is, f_{LH} takes three unique analytical approximations. As will be shown in this article, often its solution falls in between two approximations and must be solved numerically using Equation 1. The three approximations for f_{LH} are: (a) $(f_{ce}f_{cH+})^{1/2}$ when $f_{pe}/f_{ce} > 1$ and typically seen as the lower frequency edge of broadband whistler-mode hiss in Earth's magnetosphere, (b) f_{pH+} when $\sim 10^{-1} < f_{pe}/f_{ce} < \sim 1$, for example, at Saturn's topside ionosphere as measured by the Cassini spacecraft (Persoon et al., 2019; Sulaiman et al., 2017), and (c) f_{cH+} when $f_{pe}/f_{ce} < \sim 10^{-2}$, for example, in Jupiter's inner magnetosphere as measured by the Juno spacecraft and discussed in this article. The latter represents

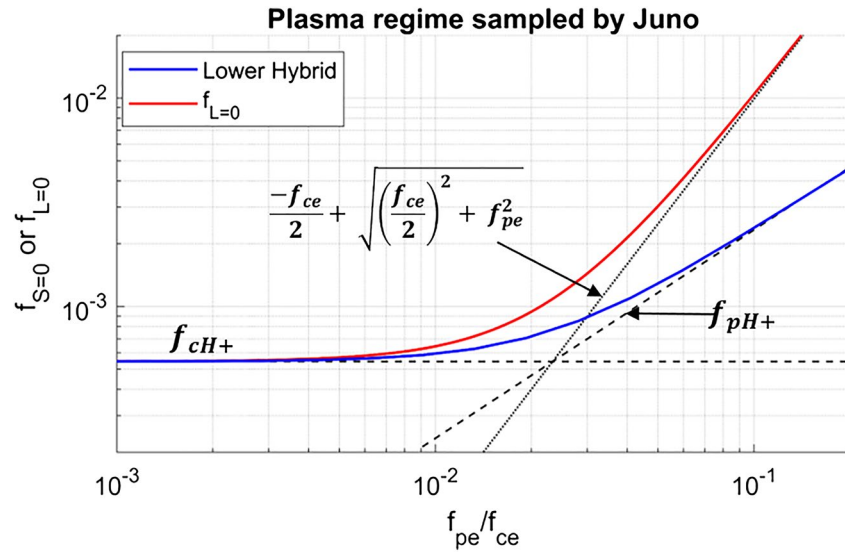


Figure 2. Same as Figure 1 but focused on the regime explored by Juno around its perijove.

maximum electric field spectral density, useful for narrowband emissions like plasma oscillations or upper hybrid emissions) for each record in the selected interval. The “top” mode finds the frequency where the spectral density slope is most sharply decreasing with increasing frequency, as for the upper cutoff of an emission. Conversely, the “bottom” mode finds where the spectral density slope is most sharply increasing with increasing frequency, as for the lower cutoff of the whistler-mode or ordinary-mode. The “manual” mode finds the geometric middle of the box frequency range where the spectral density slopes are too weak for the algorithm to identify.

Figure 3 shows frequency-time spectrograms of electric and magnetic field spectral densities during four perijoves (PJ). These events correspond to when Juno crossed the high-latitude extension of the Io torus and plasma sheet by crossing magnetic field lines connected to those regions of the inner and middle magnetosphere (Elliott et al., 2021). Overlaid on each is f_{cH+} (solid black line) calculated from the magnetic field magnitude as measured by the tri-axial fluxgate magnetometer (Connerney et al., 2017). The ultra-high magnetic field of Jupiter’s inner magnetosphere means f_{cH+} is upshifted to within the frequency range of the search coil magnetometer (lower frequency roll-off of 50 Hz). To our knowledge, this is the only region of any planetary magnetosphere where the bulk of the Alfvénic frequency range ($<f_{cH+}$) is captured by the search coil magnetometer, whereas traditionally it is well within the lower frequency range of fluxgate magnetometers (Sulaiman et al., 2020). For each of the spectrograms in Figure 3, the magnetic field does not change appreciably as shown by the f_{cH+} line. Thus, changes in the density lead to changes in f_{pe}/f_{ce} , and the characteristic frequencies vary as a result, as shown in Figure 2.

Juno’s crossing of magnetic field lines connected to the inner boundary of the Io torus is characterized by a sharp density gradient (Bagenal & Dols, 2020). This takes place at M-shell ≈ 5.9 , which is the magnetic field line connected to the equator at $\sim 5.9 R_J$ (Jupiter equatorial radius = 71,492 km). In Figure 3, this boundary is clearly identifiable at 09:30:12 (PJ5), 14:32:46 (PJ11), 04:50:40 (PJ14). Both the electric and magnetic field spectra exhibit sharp rises in the upper frequency cutoff of broadband emissions. These broadband emissions also have a distinct lower frequency cutoff at f_{cH+} , and often deviates from f_{cH+} to higher frequencies but never below. These broadband emissions are most likely in the whistler-mode, which have a theoretical upper cutoff at the lower of the electron cyclotron and plasma frequencies, that is, $\min\{f_{ce}, f_{pe}\}$ and cannot propagate below the lower hybrid frequency, f_{LH} , where they are reflected. Since f_{ce} far exceeds the frequency range shown, at $\sim 5 \times 10^6$ Hz, the upper cutoff is close to or at f_{pe} . Despite the presence of appreciable power in the magnetic field component, the broadband waves are observed to become increasingly quasi-electrostatic as they approach the lower frequency edge.

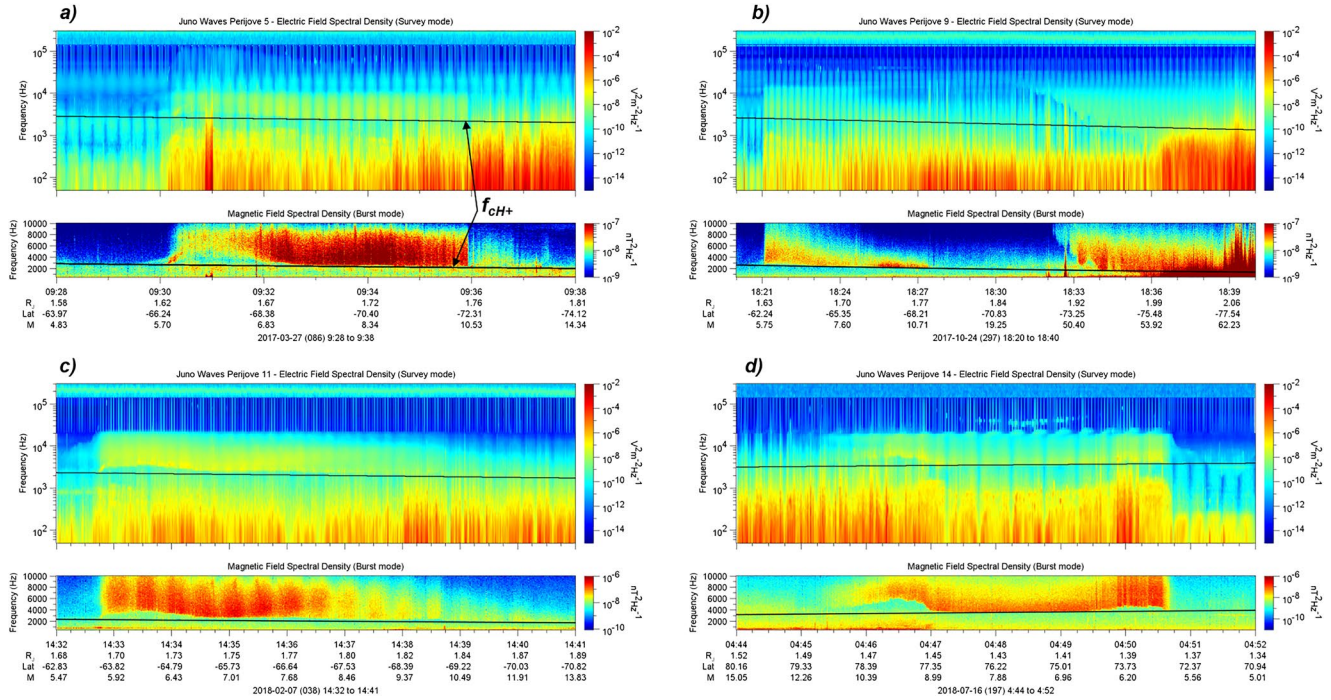


Figure 3. Electric and magnetic frequency time spectrograms during (a) PJ5 outbound, (b) PJ9 outbound, (c) PJ11 outbound, and (d) PJ14 inbound. The solid black line is the proton cyclotron frequency, denoted by f_{CH+} . A clear flux tube crossing of the Io footprint tail can be seen in (a) at ~09:31.

Recalling from Figure 2, f_{LH} is approximated as f_{CH+} or some value above. We therefore interpret the continuous lower cutoff of the broadband emissions at f_{CH+} and above as f_{LH} . Where the deviations from f_{CH+} occur, we can use Equation 1 to numerically solve for f_{pe} . This is shown during PJ5 in Figure 4a, where the

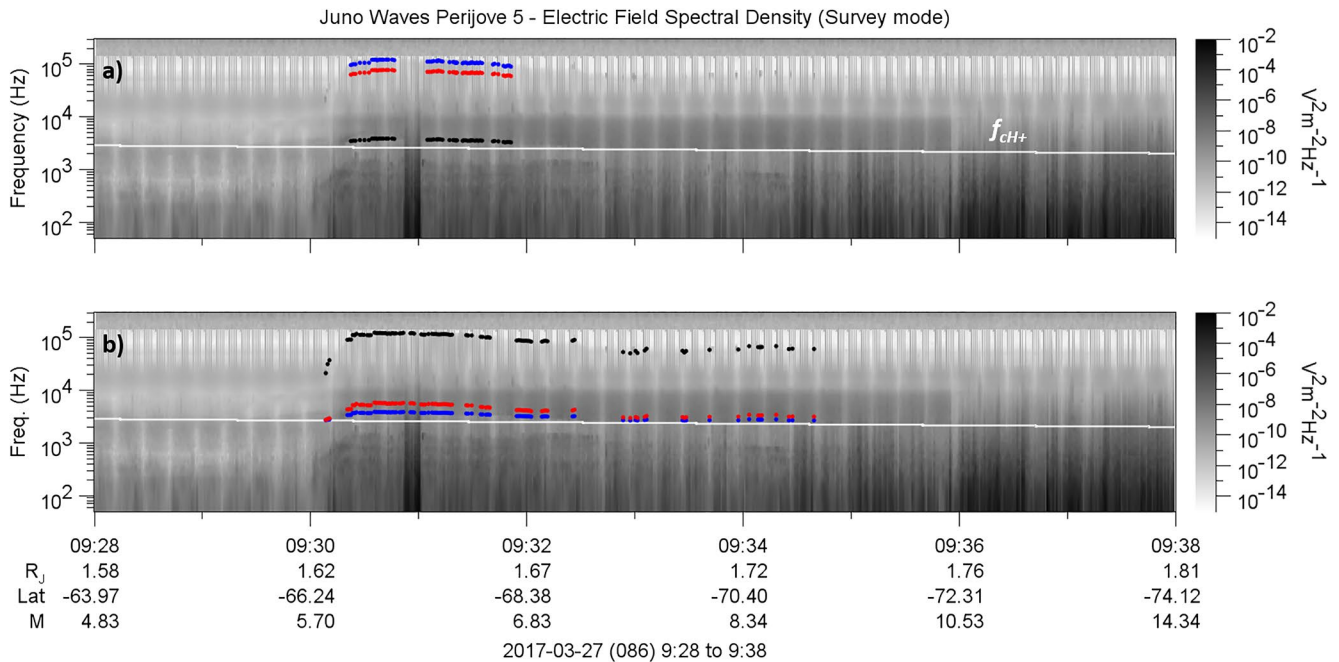


Figure 4. Electric field frequency-time spectrogram during PJ5. Digitized frequencies are represented by black dots and are f_{LH} (a) and f_{pe} (b). Blue dots are computed frequencies from solving $S = 0$ (Equation 1) and are f_{pe} (a) and f_{LH} (b). Red dots are computed frequencies from solving $L = 0$ (Equation 2) and are f_{pe} (a) and $f_L = 0$ (b).

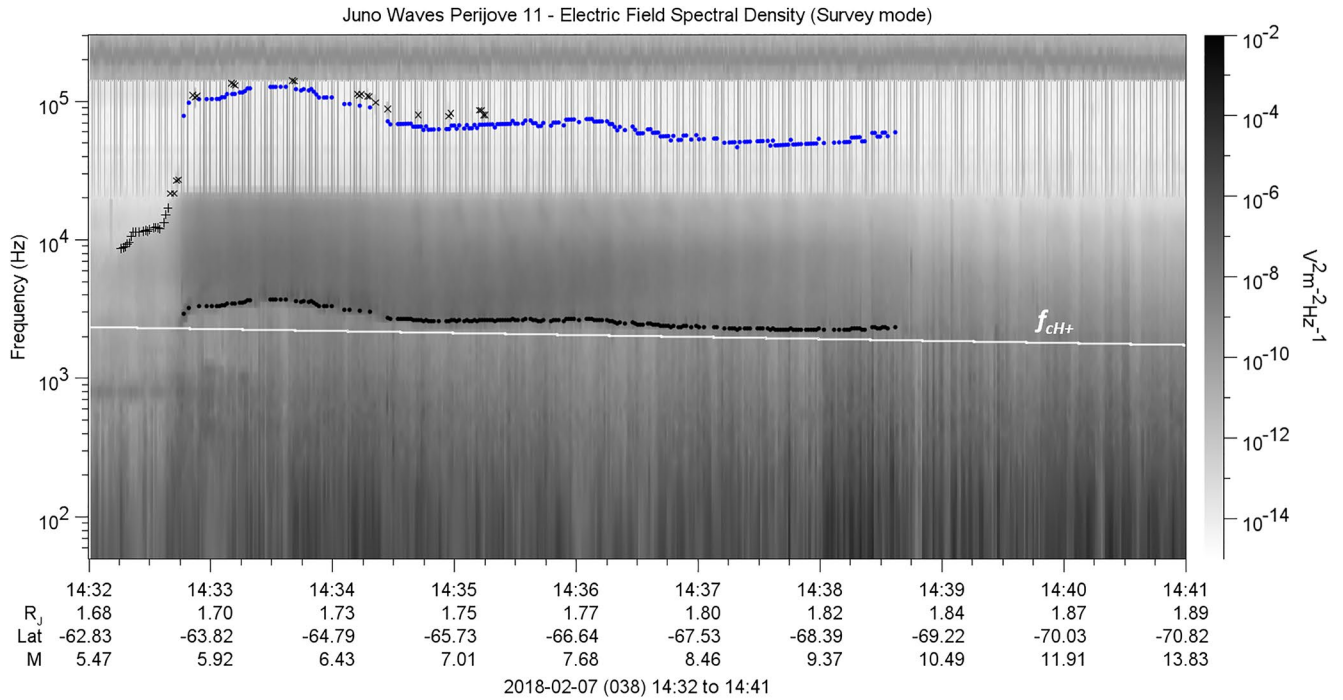


Figure 5. Electric field frequency-time spectrogram during PJ11. Black dots represent digitized frequencies as f_{LH} and blue dots are computed f_{pe} from solving $S = 0$ (Equation 1). Black crosses are digitized f_{pe} from the upper cutoff of whistler-mode emissions (before 14:33) and plasma oscillations (after 14:33).

lower cutoff (deviated from f_{cH+}) is digitized as f_{LH} , as shown by the black points. Note, where the cutoff is exactly at f_{cH+} , we cannot assign the frequency to f_{LH} since Equation 1 returns a singularity, that is, $f^2 - f_{cH+}^2$ approaches zero in the denominator. The computed f_{pe} , using Equation 1, is represented by the blue dots and it is indeed aligned with the upper cutoff of the broadband emission, consistent with the whistler mode. That said, the Z-mode is also a candidate for the broadband emission, particularly since its lower frequency cutoff, $f_L = 0$, also approximates f_{cH+} and can deviate from it, as shown in Figure 2. By assigning the digitized lower cutoff (black points) as $f_L = 0$, we use Equation 2 to solve for f_{pe} . Shown as the red points, this places f_{pe} markedly below the upper cutoff, thereby making the broadband emission unlikely to be the Z-mode.

In reverse, Figure 4b digitizes the upper frequency cutoff (black points), as well as some clear and discrete plasma oscillations (likely thermal Langmuir waves) later and assigns it as f_{pe} . The computed outputs are f_{LH} as blue points and $f_L = 0$ as red points and it is shown that throughout the time period, the computed f_{LH} consistently overlaps with the lower cutoff. This event is especially important because n_e can be inferred from the whistler-mode emission by digitizing two frequencies: f_{pe} as the upper cutoff and f_{LH} as the lower cutoff to independently compute n_e . We have shown that these two methods are in excellent agreement.

Figures 3c and 5 similarly show a broadband whistler-mode emission during PJ11. However, there is no clear upper cutoff for an extended period, although some plasma oscillations are present after 14:33. These are digitized as black crosses, in addition to the short and clear upper cutoff of the whistler mode just before the boundary crossing at 14:33 where the M-shell ≈ 5.9 . There is a long, continuous deviation of the lower cutoff from the f_{cH+} spanning 14:33 to 14:39. This is digitized as f_{LH} (black dots) and used to compute f_{pe} by numerically solving Equation 1, and there is very good agreement during times where coincident f_{pe} is identified by plasma oscillations.

Figures 3d and 6a are another example of a broadband whistler-mode emission during PJ14. Here, deviations of the lower cutoff from f_{cH+} are digitized and used to compute f_{pe} (blue dots). These are during two intervals starting at just before 04:46 and 04:50. In between these intervals, the lower cutoff is mostly at f_{cH+} , making this method of computing f_{pe} not possible. However, discrete plasma oscillations are present up to $\sim 04:50:45$ and a clear upper cutoff of the whistler mode is present thereafter—both assigned as f_{pe} (black crosses). Short overlaps between the plasma oscillations and times when f_{pe} can be computed from f_{LH} show

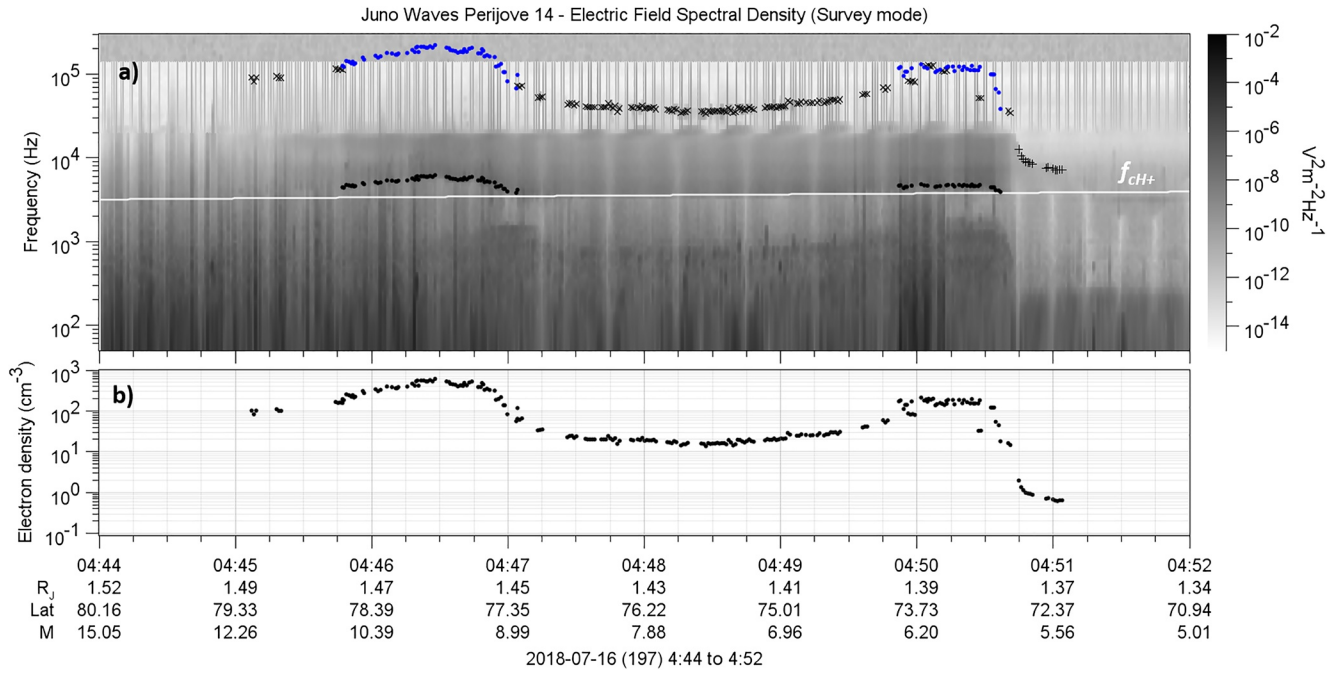


Figure 6. (a) Electric field frequency-time spectrogram during PJ14. Black dots represent digitized frequencies as f_{LH} and blue dots are computed f_{pe} from solving $S = 0$ (Equation 1). Black crosses are digitized f_{pe} from plasmas oscillations up to ~04:40:45 and from the upper cutoff of the whistler mode thereafter. (b) Inferred electron density profile from spectrogram.

that they are in agreement. Altogether, these three methods produce a continuous profile of the electron density throughout the time period, as shown in Figure 6b.

Figures 3b and 7 show a broadband emission during PJ9. This has a clear lower cutoff between 18:31 and 18:36. However, as shown in Figure 1, neither f_{LH} nor $f_L = 0$ can have a value lower than f_{cH+} , thus uniquely identifying this emission as the ordinary mode since both the whistler- and Z-modes are unlikely candidates. The ordinary mode has a lower cutoff at the plasma frequency, allowing for a direct inference of the electron density. This technique has been used in Jupiter's outer magnetosphere, utilizing low-frequency cutoff of trapped continuum radiation (Barnhart et al., 2009; Gurnett et al., 1980).

For completeness, Figure 8 shows an event when Juno was much farther out in Jupiter's magnetosphere at $>10 R_j$. Here, the combination of Jupiter's decaying magnetic field strength with radial distance and the presence of a dense plasma sheet in the equatorial region yields $f_{pe}/f_{ce} > 1$. The spectrum in Figure 8 shows a series of narrowband emissions between harmonics of f_{ce} . Similar emissions at Earth have been studied extensively by several authors (e.g., Ashour-Abdalla & Kennel, 1978; Hubbard & Birmingham, 1978). They are sometimes referred to as electron cyclotron harmonic (ECH) emissions or $(n + 1/2)f_{ce}$ bands although they do not necessarily occur at exactly half-harmonics. As discussed by Hubbard and Birmingham (1978), the ratios of cold to hot electron densities ($n_{e,c}/n_{e,h}$) and their temperatures ($T_{e,c}/T_{e,h}$) are important in determining which and how many of the bands appear. The bands may only be seen in the lowest $(3/2)f_{ce}$ band or sometimes several. If $n_{e,c}/n_{e,h}$ is large, there may be an emission near f_{UH} as is the case in Figure 8 near 55 kHz. Kurth et al. (1979) showed that an intense band often occurs when $f_{UH} \sim (n + 1/2)f_{ce}$. The presence of a bright narrowband emission above f_{ce} is possibly an upper hybrid resonance emission and can be digitized as f_{UH} . In this regime, as shown in Figure 1, $f_{UH} \approx f_{pe}$ if n is large allowing for the determination of the electron number density. Even for small n , f_{pe} can be from $f_{UH}^2 = f_{pe}^2 + f_{ce}^2$ given f_{ce} can be determined from magnetometer measurements of $|B|$. In this case, f_{UH} yields an electron density of $\sim 35 \text{ cm}^{-3}$. Kurth et al. (2015) discuss some of the uncertainties in interpreting the ECH spectrum and identifying the f_{UH} band.

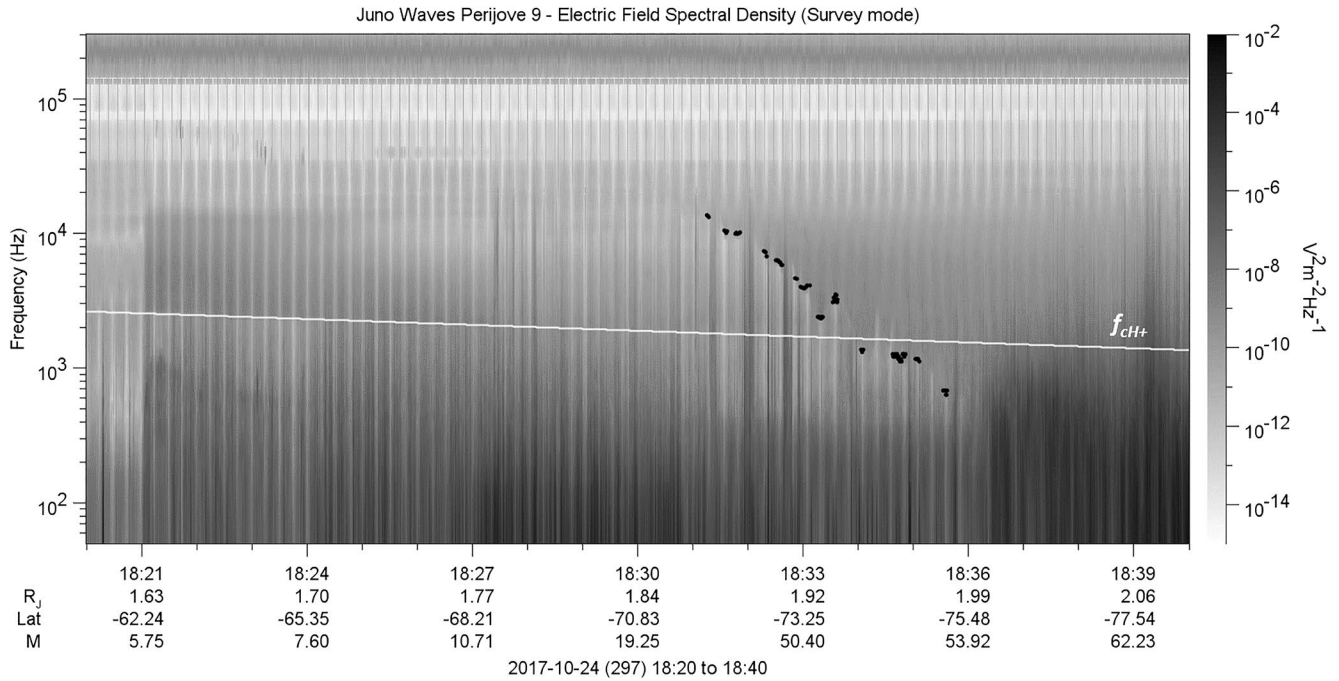


Figure 7. Electric field frequency-time spectrogram during PJ9. Black dots represent digitized frequencies as f_{pe} as the lower cutoff of the ordinary mode emission.

2.3. Uncertainty and Accuracy of Derived Electron Densities

There are three sources of error in determining n_e from the plasma wave spectrum. The first is the spectral resolution of the instrument, which translates to a density resolution through the relationship $(\Delta f/f)^2 = \Delta n_e/n_e$. For example, at ~ 60 kHz, the spectral resolution of 2% translates to a density uncertainty of 4%.

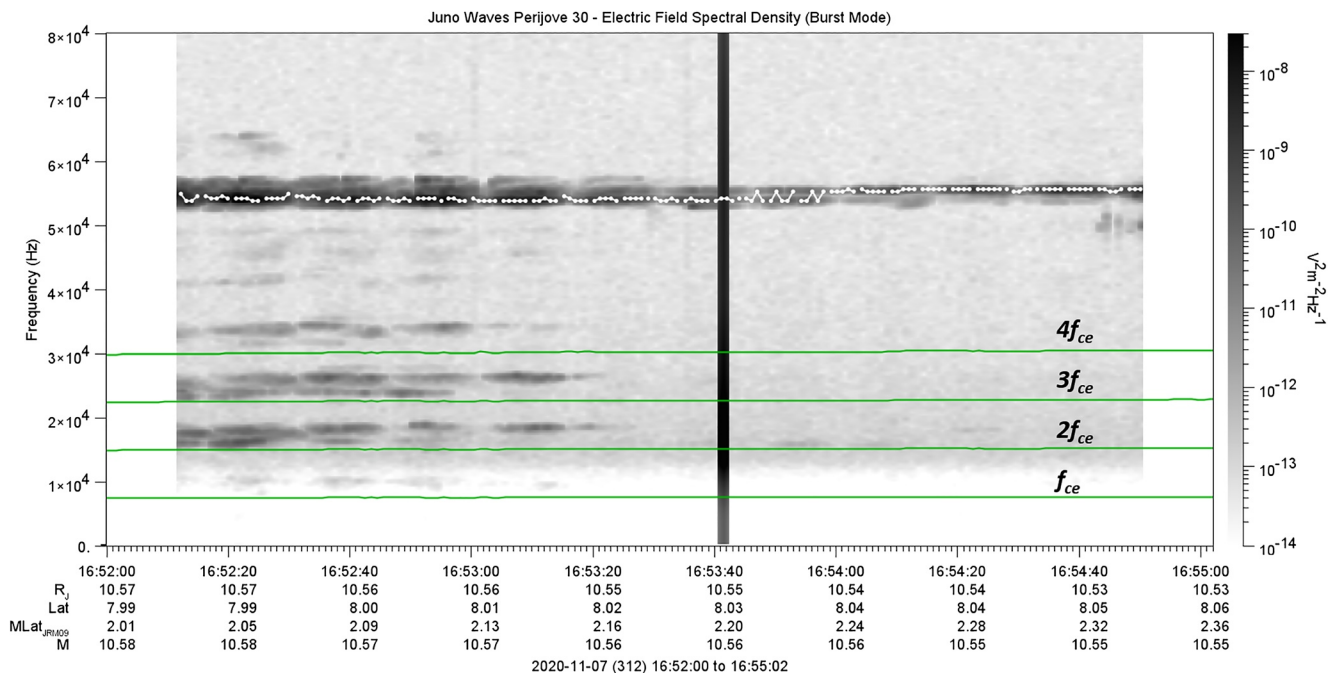


Figure 8. Electric field frequency-time spectrogram during PJ30. White dots represent digitized upper hybrid frequencies f_{UH} . Green lines are the first to fourth harmonics of f_{ce} .

The second arises from selecting the frequency at which the spectral density slope occurs. For example, the “bottom” mode (Section 2.2) is employed to identify where the spectral density slope most sharply increases with increasing frequency—corresponding to a lower frequency cutoff in the spectrogram. However, this slope is not step-like but spans over a finite frequency range, up to ~ 500 Hz. This mode is used to assign f_{LH} and given the nature of Equation 1, small changes in f_{LH} can lead to large changes in f_{pe} . The width of the slope varies throughout an event and although the associated error could occasionally exceed 50%, the frequency at which the slope is sharpest is well constrained majority of the time.

The third source of error stems from assuming that protons are the only ions that make up the quasi-neutral plasma. Unlike f_{UH} , f_{LH} is sensitive to the ion composition and a presence of heavy ions contribute to its value when solving for $S = 0$. Extending Equation 1, we have

$$S = 1 - \sum_s \frac{f_{\text{ps}}^2}{f^2 - f_{\text{cs}}^2} = 1 - \frac{f_{\text{pe}}^2}{f^2 - f_{\text{ce}}^2} - \frac{f_{\text{pH}^+}^2}{f^2 - f_{\text{cH}^+}^2} - \sum_i \frac{f_{\text{pi}}^2}{f^2 - f_{\text{ci}}^2} = 0 \quad (5)$$

where i denotes heavy ion species. Assuming a proton-electron plasma can underestimate the computed f_{pe} where heavy ions are present. For example, assuming the ions are composed of 10% H_3^+ leads to 8% change in n_e , 10% O^+ leads to 10% change in n_e , and a combination of 10% H_3^+ and 10% O^+ leads to 20% change in n_e . These do not necessarily represent the ion composition in the high-latitude regions and are merely chosen as examples. The relative abundances of heavy ions have yet to be resolved by Juno’s plasma instruments. That said, heavy ions of iogenic origin are more affected by the centrifugal forces of Jupiter’s magnetosphere and are more bound to the equator. Furthermore, the agreements between the computed f_{pe} from f_{LH} and the other independent methods to determine f_{pe} , as outlined above, lend credence to the assumption that the plasma ions are predominantly protons in the high-latitude extensions of the Io torus. If the relative abundances of heavy ions become available, Equation 3 can be used in the same manner as Equation 1.

3. Summary

We have presented a description of the methods used to derive the local electron density of the analysis of plasma wave spectra recorded by Juno/Waves. We particularly focus on the ultra-highly magnetized regime in the near-Jupiter region, that is, $f_{\text{pe}}/f_{\text{ce}} \ll 1$. Here, the plasma frequency cannot be computed by upper hybrid resonance emission lines and we therefore utilize the lower frequency edge of broadband whistler-mode radiation, as the lower hybrid frequency, to infer the electron number density. We further find the electron densities inferred from the lower hybrid frequencies to be in excellent agreement with digitized electron plasma frequencies, where available. In order to develop a useful and reliable electron density data set, a tool has been developed using Autoplot (<http://autoplot.org>), which accommodates the various methods outlined in this article.

Data Availability Statement

The Waves and MAG data used in this article have the Data set ID JNO-E/J/SS-WAV-3-CDR-BSTFULL-V1.0 and JNO-J-3-FGM-CAL-V1.0, respectively and are publicly accessible through the Planetary Plasma Interactions Node in the Planetary Data System (<https://pds-ppi.igpp.ucla.edu/>). In this article, the authors use an effective E-field antenna length of 0.5 m.

Acknowledgments

The research at the University of Iowa was supported by NASA through contract 699041X with the Southwest Research Institute. The authors are grateful to O. Santolik for useful discussions.

References

- Ashour-Abdalla, M., & Kennel, C. F. (1978). Multi-harmonic electron cyclotron instabilities. *Geophysical Research Letters*, 5(8), 711–714. <https://doi.org/10.1029/GL005i008p00711>
- Bagenal, F., & Dols, V. (2020). The space environment of Io and Europa. *Journal of Geophysical Research: Space Physics*, 125(5), e2019JA027485. <https://doi.org/10.1029/2019JA027485>
- Barnhart, B. L., Kurth, W. S., Groene, J. B., Faden, J. B., Santolik, O., & Gurnett, D. A. (2009). Electron densities in Jupiter’s outer magnetosphere determined from Voyager 1 and 2 plasma wave spectra. *Journal of Geophysical Research*, 114(A5). <https://doi.org/10.1029/2009JA014069>
- Connerney, J. E. P., Benn, M., Bjarno, J. B., Denver, T., Espley, J., Jorgensen, J. L., et al. (2017). The Juno magnetic field investigation. *Space Science Reviews*, 213(1), 39–138. <https://doi.org/10.1007/s11214-017-0334-z>

- Elliott, S. S., Sulaiman, A. H., Kurth, W. S., Faden, J., Allegrini, F., Valek, P., et al. (2021). The high-latitude extension of Jupiter's Io torus: Electron densities measured by Juno Waves. *Journal of Geophysical Research: Space Physics*, *126*, e2021JA029195. <https://doi.org/10.1029/2021JA029195>
- Gurnett, D. A., & Bhattacharjee, A. (2017). *Introduction to plasma physics: With space, laboratory and astrophysical applications* (2nd ed.). Cambridge University Press. <https://doi.org/10.1017/9781139226059>
- Gurnett, D. A., Kurth, W. S., Roux, A., Bolton, S. J., & Kennel, C. F. (1996a). Evidence for a magnetosphere at Ganymede from plasma-wave observations by the Galileo spacecraft. *Nature*, *384*(6609), 535–537. <https://doi.org/10.1038/384535a0>
- Gurnett, D. A., Kurth, W. S., Roux, A., Bolton, S. J., & Kennel, C. F. (1996b). Galileo plasma wave observations in the Io plasma torus and near Io. *Science*, *274*(5286), 391–392. <https://doi.org/10.1126/science.274.5286.391>
- Gurnett, D. A., Kurth, W. S., & Scarf, F. L. (1980). The structure of the Jovian magnetotail from plasma wave observations. *Geophysical Research Letters*, *7*(1), 53–56. <https://doi.org/10.1029/GL007i001p00053>
- Gurnett, D. A., Shawhan, S. D., & Shaw, R. R. (1983). Auroral hiss, Z mode radiation, and auroral kilometric radiation in the polar magnetosphere: DE 1 observations. *Journal of Geophysical Research*, *88*(A1), 329–340. <https://doi.org/10.1029/JA088iA01p00329>
- Hospodarsky, G. B., Kurth, W. S., Bolton, S. J., Allegrini, F., Clark, G. B., Connerney, J. E. P., et al. (2017). Jovian bow shock and magnetopause encounters by the Juno spacecraft. *Geophysical Research Letters*, *44*(10), 4506–4512. <https://doi.org/10.1002/2017GL073177>
- Hubbard, R. F., & Birmingham, T. J. (1978). Electrostatic emissions between electron gyroharmonics in the outer magnetosphere. *Journal of Geophysical Research*, *83*(A10), 4837–4850. <https://doi.org/10.1029/JA083iA10p04837>
- Kurth, W. S., Craven, J. D., Frank, L. A., & Gurnett, D. A. (1979). Intense electrostatic waves near the upper hybrid resonance frequency. *Journal of Geophysical Research*, *84*(A8), 4145–4164. <https://doi.org/10.1029/JA084iA08p04145>
- Kurth, W. S., Hospodarsky, G. B., Kirchner, D. L., Mokrzycki, B. T., Averkamp, T. F., Robison, W. T., et al. (2017). The Juno waves investigation. *Space Science Reviews*, *213*(1), 347–392. <https://doi.org/10.1007/s11214-017-0396-y>
- Kurth, W. S., Pascuale, S. D., Faden, J. B., Kletzing, C. A., Hospodarsky, G. B., Thaller, S., & Wygant, J. R. (2015). Electron densities inferred from plasma wave spectra obtained by the waves instrument on Van Allen Probes. *Journal of Geophysical Research: Space Physics*, *120*(2), 904–914. <https://doi.org/10.1002/2014JA020857>
- LaBelle, J., & Treumann, R. A. (2002). Auroral radio emissions. 1. Hisses, roars, and bursts. *Space Science Reviews*, *101*(3), 295–440. <https://doi.org/10.1023/A:1020850022070>
- Menietti, J. D., Averkamp, T. F., Ye, S.-Y., Sulaiman, A. H., Morooka, M. W., Persoon, A. M., et al. (2018). Analysis of intense Z-mode emission observed during the Cassini proximal orbits. *Geophysical Research Letters*, *45*(14), 6766–6772. <https://doi.org/10.1002/2018GL077354>
- Meredith, N. P., Horne, R. B., Thorne, R. M., & Anderson, R. R. (2003). Favored regions for chorus-driven electron acceleration to relativistic energies in the Earth's outer radiation belt. *Geophysical Research Letters*, *30*(16). <https://doi.org/10.1029/2003GL017698>
- Meyer-Vernet, N., & Perche, C. (1989). Tool kit for antennae and thermal noise near the plasma frequency. *Journal of Geophysical Research*, *94*(A3), 2405–2415. <https://doi.org/10.1029/JA094iA03p02405>
- Persoon, A. M., Gurnett, D. A., Kurth, W. S., Hospodarsky, G. B., Groene, J. B., Canu, P., & Dougherty, M. K. (2005). Equatorial electron density measurements in Saturn's inner magnetosphere. *Geophysical Research Letters*, *32*(23). <https://doi.org/10.1029/2005GL024294>
- Persoon, A. M., Kurth, W. S., Gurnett, D. A., Groene, J. B., Sulaiman, A. H., Wahlund, J.-E., et al. (2019). Electron density distributions in Saturn's ionosphere. *Geophysical Research Letters*, *46*(6), 3061–3068. <https://doi.org/10.1029/2018GL078020>
- Stix, T. H. (1992). *Waves in plasmas*. AIP-Press. Retrieved from <https://www.springer.com/gp/book/9780883188590>
- Sulaiman, A. H., Hospodarsky, G. B., Elliott, S. S., Kurth, W. S., Gurnett, D. A., Imai, M., et al. (2020). Wave-particle interactions associated with Io's auroral footprint: Evidence of Alfvén, ion cyclotron, and whistler modes. *Geophysical Research Letters*, *47*(22), e2020GL088432. <https://doi.org/10.1029/2020GL088432>
- Sulaiman, A. H., Kurth, W. S., Persoon, A. M., Menietti, J. D., Farrell, W. M., Ye, S.-Y., et al. (2017). Intense harmonic emissions observed in Saturn's ionosphere. *Geophysical Research Letters*, *44*(24), 12049–12056. <https://doi.org/10.1002/2017GL076184>